

Dynamic structure factor of liquid ^4He across the normal-superfluid transition

G. Ferré and J. Boronat*

*Departament de Física, Universitat Politècnica de Catalunya,
Campus Nord B4-B5, E-08034, Barcelona, Spain*

We have carried out a microscopic study of the dynamic structure factor of liquid ^4He across the normal-superfluid transition temperature using the path integral Monte Carlo method. The ill-posed problem of the inverse Laplace transform, from the imaginary-time intermediate scattering function to the dynamic response, is tackled by stochastic optimization. Our results show a quasi-particle peak and a small and broad multiphonon contribution. In spite of the lack of strength in the collective peaks, we clearly identify the rapid dropping of the roton peak amplitude when crossing the transition temperature T_λ . Other properties such as the static structure factor, static response, and one-phonon contribution to the response are also calculated at different temperatures. The changes of the phonon-roton spectrum with the temperature are also studied. An overall agreement with available experimental data is achieved.

PACS numbers: 67.25.dt, 02.70.Ss, 02.30.Zz

I. INTRODUCTION

The most relevant information on the dynamics of a quantum liquid is contained in the dynamic structure factor $S(\mathbf{q}, \omega)$, which is experimentally measured by means of inelastic neutron scattering.¹ Probably, superfluid ^4He has been the most deeply studied system from both theory and experiment and a great deal of information about it is nowadays accessible.² For many years, liquid ^4He was the only quantum fluid showing Bose-Einstein condensation and superfluidity until the discovery of the fully Bose-Einstein condensate in 1995.^{3,4} Therefore, the number of measures of $S(\mathbf{q}, \omega)$ at different temperatures and momentum transfer has been continuously growing, with more refined data along the years.^{5–10} The emergence of strong quasi-particle peaks going down the normal-superfluid transition ($T_\lambda = 2.17\text{ K}$) has been associated with the superfluidity of the system by application of the Landau criterium. Much of the interest on the dynamics of strongly-correlated liquid ^4He is then related to the effects on the dynamics of this second-order λ -transition.

In the limit of zero temperature, the richest and most accurate microscopic description of the dynamic response of liquid ^4He has been achieved by progressively more sophisticated correlated basis function (CBF) theory.¹¹ The development of this theory has been stimulated by the continuous improvement of the experimental resolution in inelastic neutron scattering. Recently, Campbell *et al.*¹² have incorporated three-body fluctuations in an extended CBF approach and proved a remarkable improvement of both the excitation spectrum and full $S(\mathbf{q}, \omega)$, with features not so clearly seen before and that are in nice agreement with the most recent experimental data.¹³ On the other hand, the most accurate tools to deal with ground-state properties are the quantum Monte Carlo (QMC) methods. In the case of bosons as ^4He , these methods are able to produce essentially exact results for its equation of state and structure properties which are in close agreement with experimental data.¹⁴ Importantly, QMC methods are not restricted to

the limit of zero temperature and are equally powerful to introduce the temperature as a variable through the sampling of the statistical density matrix, implemented by the path integral Monte Carlo (PIMC) method.¹⁵

QMC methods simulate quantum systems using imaginary-time dynamics since they are intended for achieving the lowest-energy state. Therefore, having no access to real-time evolution one loses the possibility of getting the dynamic structure factor by a Fourier transform of the intermediate scattering function $F(\mathbf{q}, t)$, as it happens in simulations of classical systems using Molecular Dynamics. Quantum simulations are able to sample this time-dependent function but in imaginary time τ , $F(\mathbf{q}, \tau)$, and from it to get the dynamic response through an inverse Laplace transform. But it is well known that this inverse transform is an ill-posed problem. This means, at the practical level, that the always finite statistical error of QMC data makes impossible to find a unique solution for the dynamic structure factor.

Inverse problems in mathematical physics are a long-standing topic in which elaborated regularization techniques have been specifically developed.¹⁶ Focusing on the inversion of QMC data, to extract the dynamic response, several methods have been proposed in the last years. Probably, the most used approach is the Maximum Entropy (ME) method which incorporates some a priori expected behavior through an entropic term.¹⁷ This method works quite well if the response is smooth but it is not able to reproduce responses with well-defined peaks. In this respect, other methods have recently proved to be more efficient than ME. For instance, the average spectrum method (ASM),¹⁸ the stochastic optimization method (SOM),¹⁹ the method of consistent constraints (MCC),²⁰ and the genetic inversion via falsification of theories (GIFT) method²¹ have been able to recover sharp features in $S(\mathbf{q}, \omega)$ which ME smoothed out. All those methods are essentially stochastic optimization methods using different strategies and constraints. It is also possible to work out the inverse problem without stochastic grounds²² by using the Moore-

Penrose pseudoinverse and a Tikhonov regularization.²³ Other approaches try to reduce the ill-conditioned character of this inverse problem by changing the kernel from the Laplace transform to a Lorentz one.²⁴ Finally, the computation of complex-time correlation functions has been recently realized in simple problems and proved to be able to severely reduce the ill-nature of the Laplace transform.²²

In this paper, we use the PIMC method to estimate the dynamic response of liquid ^4He in a range of temperatures covering the normal-superfluid transition at $T_\lambda = 2.17$ K. The inversion method from imaginary time to energy is carried out via the simulated annealing method, which is a well-known stochastic multidimensional optimization method widely used in physics and engineering.²⁵ Our method is rather similar to the GIFT one²¹ but changing the genetic algorithm by simulated annealing. The GIFT method was applied to the study of the dynamic response of liquid ^4He at zero temperature and proved to work much better than ME, producing a rather sharp quasi-particle peak and also some structure at large energies, corresponding to multiparticle excitations.²¹ The temperature dependence of $S(\mathbf{q}, \omega)$ has been much less studied. Apart from a quantum-semiclassical estimation of the response at high q ,²⁶ the only reported results were obtained by combining PIMC and the ME method which worked well in the normal phase but not in the superfluid part.²⁷ Therefore, the significant effect of the temperature on the dynamics of the liquid through the λ transition was lost. We show that the improvement on the inversion method leads to a significantly better description of $S(\mathbf{q}, \omega)$ in all the temperature range studied, with reasonable agreement with experimental data.

The rest of the paper is organized as follows. A short description of the PIMC method and a discussion of the inversion method used is contained in Sec. II. In Sec. III, we report the results achieved for the dynamic response, excitation spectrum, phonon strength and lowest energy-weighted sum rules across the transition. Finally, the main conclusions and a summary of the main results are contained in Sec. IV.

II. METHOD

The thermal density matrix of a quantum system is given by

$$\hat{\rho} = \frac{e^{-\beta\hat{H}}}{Z}, \quad (1)$$

where $\beta = 1/(k_B T)$, k_B is the Boltzmann constant, and $Z = \text{Tr}(e^{-\beta\hat{H}})$ is the partition function. The knowledge of $\hat{\rho}$ allows for the calculation of the expected value of any operator \hat{O} ,

$$\langle \hat{O} \rangle = \text{Tr}(\hat{\rho} \hat{O}), \quad (2)$$

which in coordinate representation turns to

$$\langle \hat{O} \rangle = \int d\mathbf{R} \rho(\mathbf{R}, \mathbf{R}; \beta) O(\mathbf{R}), \quad (3)$$

with $\mathbf{R} = \{\mathbf{r}_1, \dots, \mathbf{r}_N\}$ for an N -particle system. Deep in the quantum regime, i.e. at very low temperature, the estimation of the density matrix for a many-body system is obviously a hard problem. However, the convolution property of $\hat{\rho}$,

$$\rho(\mathbf{R}_1, \mathbf{R}_{M+1}; \beta) = \int d\mathbf{R}_2 \dots d\mathbf{R}_M \prod_{j=1}^M \rho(\mathbf{R}_j, \mathbf{R}_{j+1}; \tau), \quad (4)$$

with M an integer and $\tau = \beta/M$, shows how to build the density matrix at the desired temperature T from a product of density matrices at a higher temperature MT . If the temperature is large enough, one is able to write accurate approximations for $\hat{\rho}$ and thus the quantum density matrix can be calculated, as stated by the Trotter formula

$$e^{-\beta(\hat{K}+\hat{V})} = \lim_{M \rightarrow \infty} \left(e^{-\tau\hat{K}} e^{-\tau\hat{V}} \right)^M. \quad (5)$$

In Eq. (5), we have considered a Hamiltonian $\hat{H} = \hat{K} + \hat{V}$, with \hat{K} and \hat{V} the kinetic and potential operators, respectively. In the limit of high temperature the system approaches the classical regime where $e^{-\beta(\hat{K}+\hat{V})} = e^{-\beta\hat{K}} e^{-\beta\hat{V}}$. This factorization, called primitive approximation, is however not accurate enough to simulate a quantum liquid as ^4He because the number of required terms (*beads*) M is too large. To make our PIMC simulations of superfluid ^4He reliable, we use a fourth-order time-step (τ) approximation due to Chin, following the implementation discussed in Ref. 29. Liquid ^4He is a Bose liquid and thus we need to sample not only particle positions but permutations among them. To this end, we use the worm algorithm.³⁰

In the present work, we are mainly interested in calculating the intermediate scattering function $F(\mathbf{q}, \tau)$, defined as

$$F(\mathbf{q}, \tau) = \frac{1}{N} \langle \hat{\rho}_{\mathbf{q}}(\tau) \hat{\rho}_{\mathbf{q}}^\dagger(0) \rangle, \quad (6)$$

with $\hat{\rho}_{\mathbf{q}}(\tau) = \sum_{i=1}^N e^{i\mathbf{q} \cdot \mathbf{r}_i}$ the density fluctuation operator. The function $F(\mathbf{q}, \tau)$ is the Laplace transform of the dynamic structure factor $S(\mathbf{q}, \omega)$ which satisfies the detailed balance condition,

$$S(\mathbf{q}, -\omega) = e^{-\beta\omega} S(\mathbf{q}, \omega), \quad (7)$$

relating the response for negative and positive energy transfers ω . Taking into account Eq. (7), one gets

$$F(\mathbf{q}, \tau) = \int_0^\infty d\omega S(\mathbf{q}, \omega) (e^{-\omega\tau} + e^{-\omega(\beta-\tau)}). \quad (8)$$

The intermediate scattering function is periodic with τ , as it can be immediately seen from Eq. (8): $F(\mathbf{q}, \beta -$

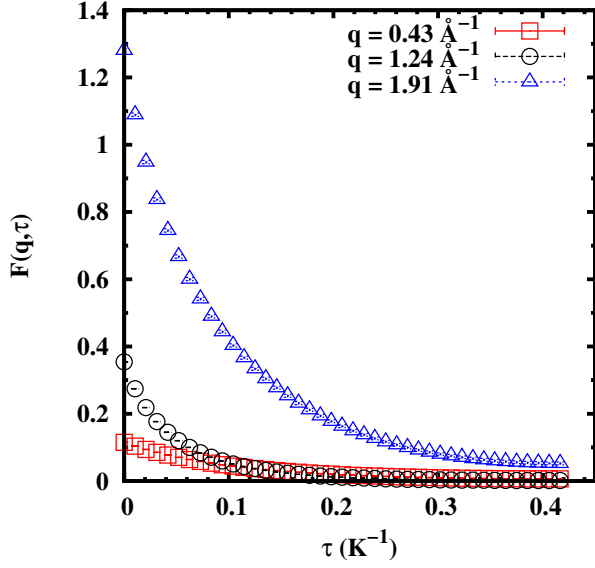


FIG. 1. (Color online) Intermediate scattering function computed for ^4He at saturated vapor pressure ($\rho = 0.021858 \text{ \AA}^{-3}$) and $T = 1.2 \text{ K}$, for different values of q .

$\tau) = F(\mathbf{q}, \tau)$. Therefore, it is necessary to sample this function only up to $\beta/2$ (half of the polymer representing each particle in PIMC terminology). From the PIMC simulation, one samples $F(\mathbf{q}, \tau)$ at the discrete points in which the action at temperature T is decomposed (Eq. 4).

In Fig. 1, we show the characteristic behavior of $F(\mathbf{q}, \tau)$ for three different q values at $T = 1.2 \text{ K}$. These are monotonously decreasing functions ending at a finite value at $T/2$ which approaches zero when $T \rightarrow 0$. The initial point at $\tau = 0$ corresponds to the zero energy-weighted sum rule of the dynamic response, which in turn is the static structure factor at that specific q value,

$$m_0 = S(\mathbf{q}) = \int_{-\infty}^{\infty} d\omega S(\mathbf{q}, \omega). \quad (9)$$

With the PIMC results for $F(\mathbf{q}, \tau)$, the next step is to find a reasonable model for $S(\mathbf{q}, \omega)$ having always in mind the ill-conditioned nature of this goal. In our scheme, we assume a step-wise function,

$$S_m(q, \omega) = \sum_{i=1}^{N_s} \xi_i \Theta(\omega - \omega_i) \Theta(\omega_{i+1} - \omega), \quad (10)$$

with $\Theta(x)$ the Heaviside step function, and ξ_i and N_s parameters of the model. As our interest relies on the study of homogeneous translationally invariant systems, the response functions depend only of the modulus q . Introducing $S_m(q, \omega)$ in Eq. (8), one obtains the corre-

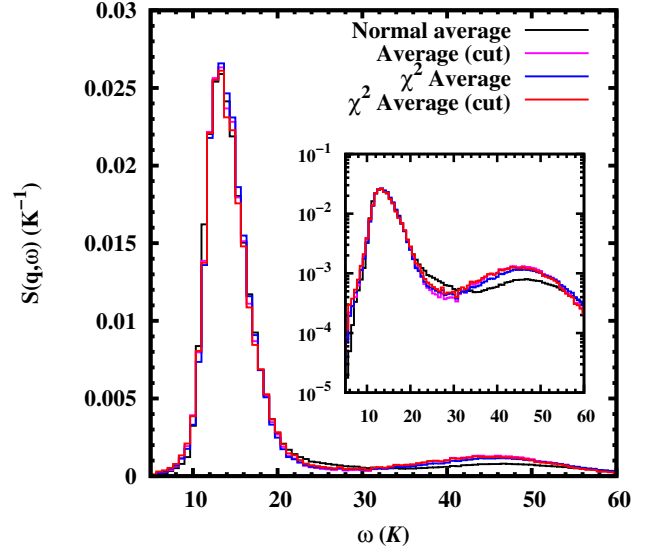


FIG. 2. (Color online) Dynamic structure factor at $T = 1.2 \text{ K}$, saturated vapor pressure (SVP), and $q = 0.76 \text{ \AA}^{-1}$ using different averaging methods. Inset shows same data but using a log scale in the y -axis.

sponding model for the intermediate scattering function,

$$F_m(q, \tau) = \sum_{i=1}^{N_s} \xi_i \left[\frac{1}{\tau} (e^{-\tau\omega_i} - e^{-\tau\omega_{i+1}}) + \frac{1}{\beta - \tau} (e^{-(\beta - \tau)\omega_i} - e^{-(\beta - \tau)\omega_{i+1}}) \right] \quad (11)$$

Written in this way, the inverse problem is converted into a multivariate optimization problem which tries to reproduce the PIMC data with the proposed model, Eq. 11. To this end, we use the simulated annealing method which relies on a thermodynamic equilibration procedure from high to low temperature according to a predefined template schedule.²⁵ The cost function to be minimized is the quadratic dispersion,

$$\chi^2(q) = \sum_{i=1}^{N_p} [F(q, \tau_i) - F_m(q, \tau_i)]^2, \quad (12)$$

with N_p the number of points in which the PIMC estimation of the intermediate scattering function is sampled. Eventually, one can also introduce as a denominator of Eq. (12) the statistical errors coming from the PIMC simulations. However, we have checked that this is not affecting so much the final result since the size of the errors is rather independent of τ .

The optimization leading to $S(q, \omega)$ is carried out over a number N_t of independent PIMC calculations of $F(q, \tau)$. Typically, we work with a population $N_t = 24$ and for each one we perform a number $N_a = 100$ of independent simulated annealing searches. The mean average of these N_a optimizations is our prediction for the dynamic response for a given $F(q, \tau)$. We also register the

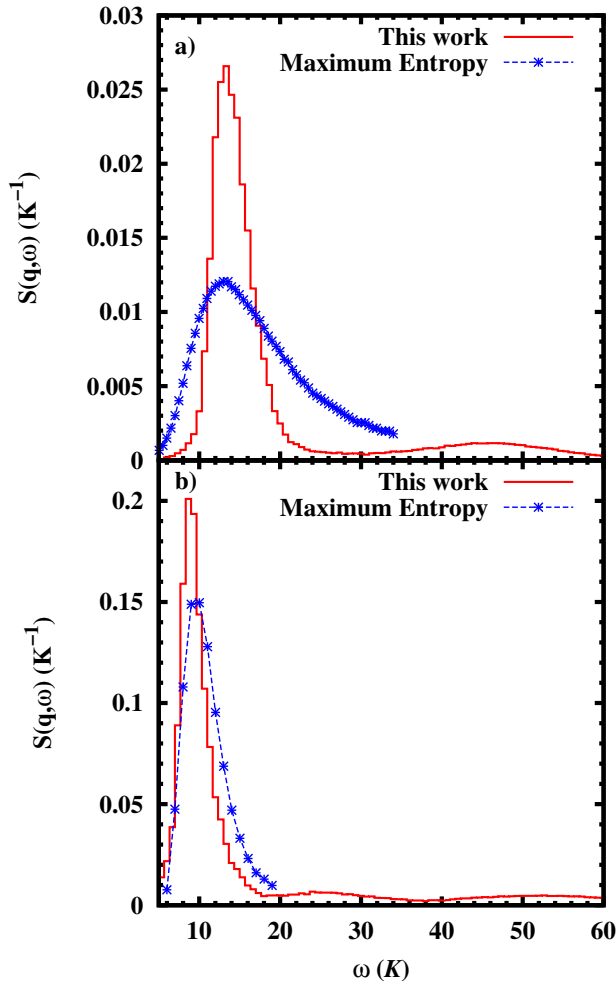


FIG. 3. (Color online) Comparison between the present results for the dynamic structure factor and those obtained in Ref. 27 using the maximum entropy method for $q = 0.76 \text{ \AA}^{-1}$ (a) and 1.81 \AA^{-1} (b). Both results are calculated at SVP and $T = 1.2 \text{ K}$.

mean value of χ^2 (Eq. 12) of the N_a optimizations. As an example, the mean value of χ^2 in a simulation with data at $T = 1.2 \text{ K}$ and $q = 1.91 \text{ \AA}^{-1}$ is $2.19 \cdot 10^{-5}$, with minimum and maximum values of $2.37 \cdot 10^{-6}$ and $3.80 \cdot 10^{-4}$, respectively. At this same temperature, $N_p = 41$ and the number of points of the model $S(q, \omega)$ (Eq. 11) is $N_s = 150$.

With the outcome for the N_t series we have tried different alternatives to get the final prediction. We can take just the statistical mean of the series or a weighted mean, in which the weight of each function is the inverse of its corresponding χ^2 , to give more relevance to the best-fitted models. Additionally, we have also tried to make both of these estimations but selecting the 20% best functions according to its χ^2 . In Fig. 2, we plot the results obtained following these different possibilities. All the results are quite similar, with minor differences; only at large energies we can observe that the weighted mean

gives slightly more structure (see inset in Fig. 2). Also, the effect of selecting the best χ^2 models seems to be not much relevant.

In Fig. 3, we compare the results obtained for the dynamic structure factor at $T = 1.2 \text{ K}$ and saturated vapor pressure (SVP) with previous results obtained using the Maximum Entropy (ME) method.²⁷ The ME results are significantly broader, mainly at the lowest q value, and with only smooth features. This broadening is probably a result of the entropic prior used in those estimations, which seems to favor smooth solutions. In the figure, we can observe that the position of the ME peak is coincident with ours but the ME solution lacks of any structure beyond the quasi-particle peak (see Appendix for additional comparisons between ME and our stochastic optimization procedure). In our estimation, we do not use any prior information in the search of optimal reconstructions and thus it is free from any a priori information except that the function is positive definite for any energy. Moreover, the simulated annealing optimization leads to dynamic responses that fulfil the energy-weighted sum rules m_0 and m_1 ,

$$m_1 = \int_{-\infty}^{\infty} d\omega \omega S(q, \omega) = \frac{\hbar^2 q^2}{2m}, \quad (13)$$

without imposing them as constraints in the cost function (Eq. 12). Also, the m_{-1} sum-rule, related to the static response, is in agreement with experiment (see next Section).

III. RESULTS

We have performed PIMC calculations of liquid ^4He following the SVP densities, from $T = 0.8$ to 4 K . The interatomic potential is of Aziz type³¹ and the number of particles in the simulation box, under periodic boundary conditions, is $N = 64$. In some cases we have used a larger number of particles ($N = 128$) without observing any significant change in $F(q, \tau)$. The number of terms M (Eq. 4) is large enough to eliminate any bias coming from the path discretization; we used $\tau = 0.0104 \text{ K}^{-1}$.

We compare our result for the dynamic response in the superfluid phase with experimental data from Ref. 5 in Fig. 4. The theoretical peak is located around an energy which is very close to the experimental one but it is still broader than in the experiment. However, the strength (area) of this peak is in good agreement with the experimental one, as we will comment later. The quasi-particle peak disappears in the normal phase, above T_λ , as we can see in Fig. 5. In this figure, we compare our results at $T = 4 \text{ K}$ with experimental outcomes at the same T . In this case, we see that both the position of the peak and its shape is in an overall agreement with the experiment.

One of the main goals of our study has been the study of the effect of the temperature on the dynamics of liquid ^4He . In Fig. 6, we report results of $S(q, \omega)$ in a range

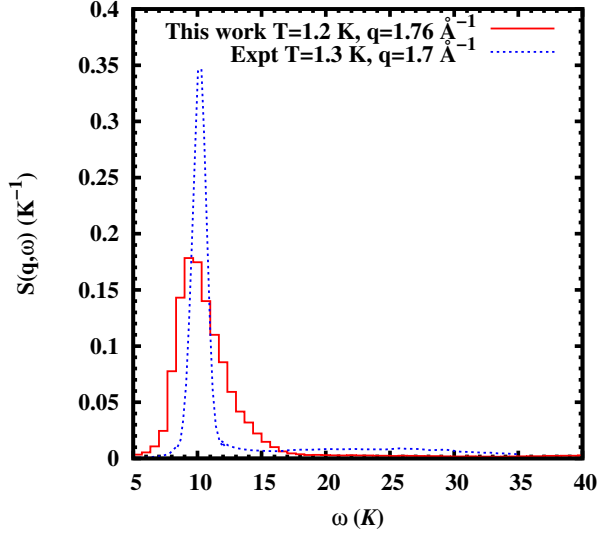


FIG. 4. (Color online) Dynamic structure factor at $T = 1.2$ K and $q = 1.76 \text{ \AA}^{-1}$ compared with experimental data ($T = 1.3 \text{ K}$, $q = 1.7 \text{ \AA}^{-1}$).⁵

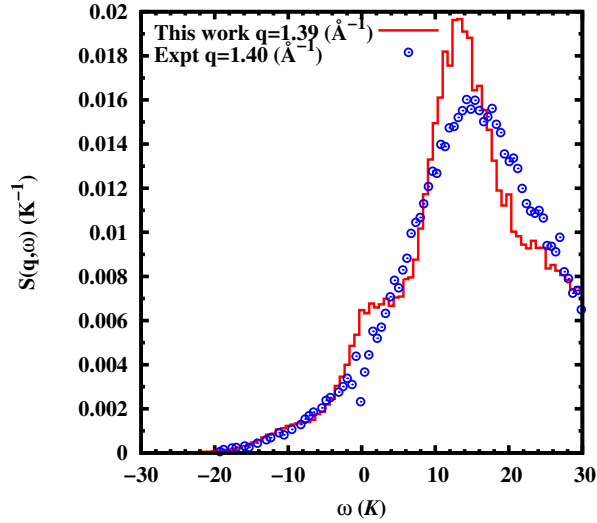


FIG. 5. (Color online) Dynamic structure factor at $T = 4.0$ K and $q = 1.40 \text{ \AA}^{-1}$. The experimental data is from Ref. 32.

of temperatures from $T = 0.8$ to 4 K in the phonon region of the spectrum, with $q = 0.88 \text{ \AA}^{-1}$. At this low q value, the behavior with T is not much different for the superfluid and normal phases, a feature which is also observed in neutron scattering data.² We observe a progressive broadening of the peak with T which appears already below T_λ and continues above it. Even at the highest temperature $T = 4$ K, we identify a collective peak corresponding to a sound excitation.² The main difference between both regimes is that the quasi-particle energy below T_λ is nearly independent of T whereas, in the normal phase, this energy decreases in a monotonous

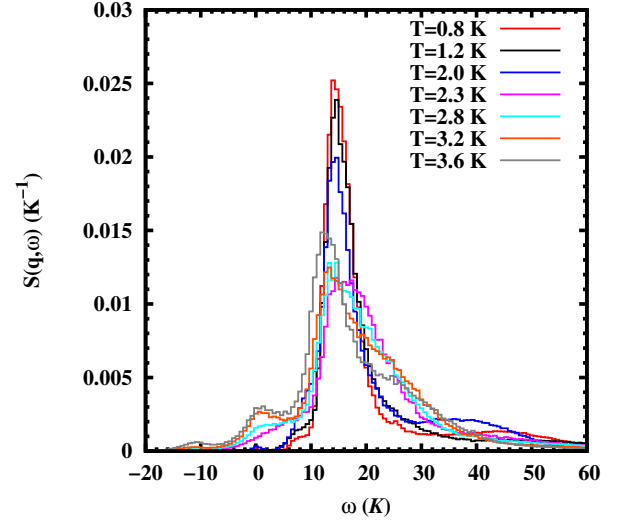


FIG. 6. (Color online) Dynamic structure factor of liquid ^4He for $q = 0.88 \text{ \AA}^{-1}$ at different temperatures.

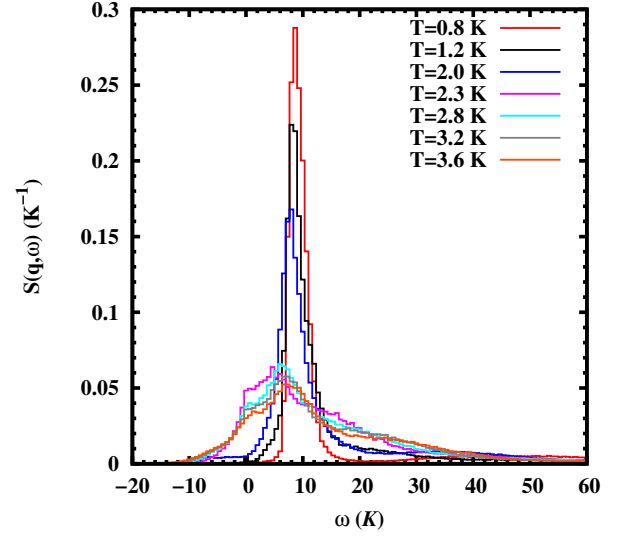


FIG. 7. (Color online) Dynamic structure factor of liquid ^4He for $q = 1.91 \text{ \AA}^{-1}$ at different temperatures.

way.

Near the roton, the dependence of the dynamic response with T is significantly different. In Fig. 7, we report results of $S(q, \omega)$ at $q = 1.91 \text{ \AA}^{-1}$ at different temperatures across T_λ . The most relevant feature is the drop of the quasi-particle peak for $T > T_\lambda$. In the superfluid phase, the peak remains sharp with a nearly constant energy. Just crossing the transition (in our data for $T \geq 2.3$ K), the peak disappears and only a broad response is observed, with an energy that moves slightly down. According to the Landau criterium the existence of a roton gap implies a critical velocity larger than zero and thus a superfluid phase. Our PIMC data is consistent

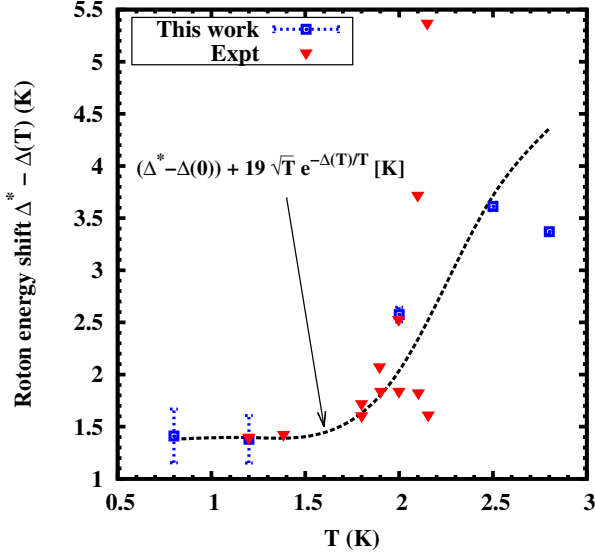


FIG. 8. (Color online) Temperature dependence of the roton energy. The experimental points and suggested fit are from Ref. 33 with $\Delta(0) = 8.62$ K. In the fit, $\Delta^* > \Delta(T)$ stands for an arbitrary energy value.

with this picture since we observe as the resulting superfluid density, derived from the winding number estimator, goes to zero at T_λ , in agreement with the disappearance of the roton excitation in $S(q, \omega)$.

Our results for the temperature dependence of the roton energy $\Delta(T)$ are shown in Fig. 8. For temperatures $T < 1.5$ K, $\Delta(T)$ is practically constant around a value 8.60 K, in agreement with experiment.³³ For larger temperatures, still in the superfluid part, this energy gap starts to decrease with the largest change around the transition temperature. For temperatures $T > 2.5$ K, the peak vanishes and $\Delta(T)$ flattens but then one really can not continue speaking about the roton mode. In the same figure we report experimental results for the roton energy in the superfluid phase. At same temperature, our results agree well with the experimental ones which show some erratic behavior around $T \simeq 2$ K but compatible with a decrease of the roton gap with T . Still in the same figure, we report the fit used in Ref. 33, that is based on the roton-roton interaction derived from Landau and Khalatnikov theory.³⁴ This law seems to be right only at the qualitative level, with significant deviation with our results and still larger discrepancies with the experimental values.

The results obtained for $S(q, \omega)$ in the present calculation are summarized in Fig. 9 as a color map in the momentum-energy plane. In the superfluid phase, the phonon-roton curve is clearly observed, with the highest strength of the quasi-particle peak located in the roton minimum, in agreement with experiment. The multiparticle part above the single-mode peak is also observed but without any particular structure. At $T = 2$ K the roton peak is still observed but some intensity starts to appear

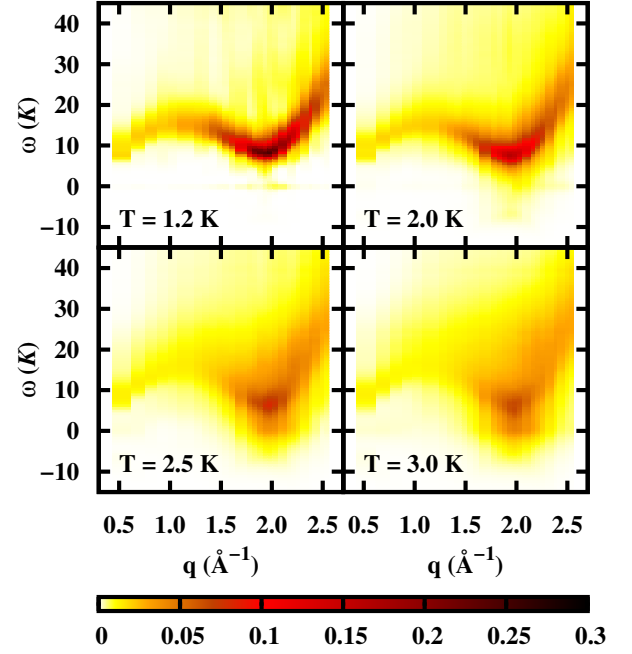


FIG. 9. (Color online) Color map of the dynamic response in the momentum-energy plane at different temperatures, below and upper T_λ .

below it. At $T = 2.5$ and 3 K, we still obtain intensity in the roton but the peak, and in general, all the spectrum appears much more diffuse.

The excitation energy of the collective mode is shown in Fig. 10 at different temperatures. Our results at the lowest temperatures, $T = 0.8$ and 1.2 K, are indistinguishable within the statistical errors and are in close agreement with the inelastic neutron scattering data at $T = 1.2$ K from Refs. 35 and 36, except at the end of the spectrum (Pitaevskii plateau). In fact, for $q > 2.5 \text{ \AA}^{-1}$ the dynamic response that we obtain from the reconstruction of the imaginary-time intermediate scattering function is rather broad and one can not distinguish the double peak structure observed in experiments. Also, notice that the energies corresponding to $q \lesssim 0.5 \text{ \AA}^{-1}$ are not accessible in our simulations since our minimum q_{\min} value is restricted to be $2\pi/L$, with L the length of the simulation box. At $T = 2$ K, very close to the superfluid transition temperature, we observe as the energies of the maxon and roton modes significantly decrease whereas the phonon part is less changed. When the temperature is above the transition, we can observe that the maximum of the peaks, now much broader, seem to collapse again in a common curve around the maxon. Instead, in the roton it seems that the energy could increase again at the largest temperature. This latter feature is quite unexpected and could be a result of our difficulty in the localization of the maximum in a rather broad dynamic response. The overall description on the evolution of the phonon-roton spectrum with T is in close agreement with

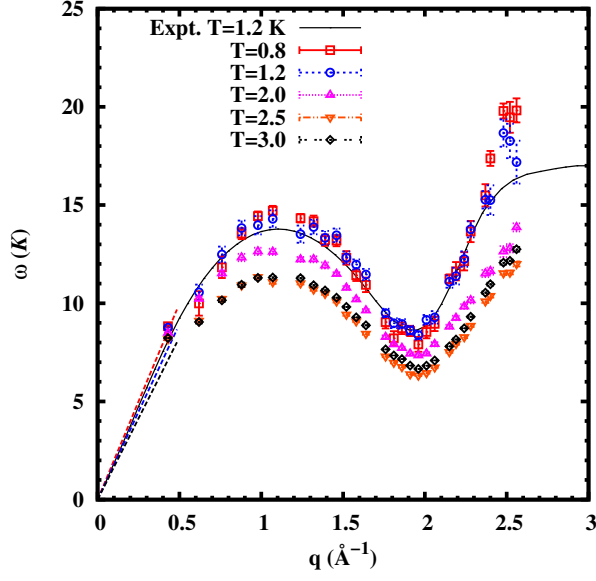


FIG. 10. (Color online) Phonon-roton spectrum of liquid ^4He at different temperatures. The line corresponds to experimental data at $T = 1.2$ K.^{35,36} Straight lines at small q stand for the low q behavior, $\omega = cq$ with c the speed of sound, at temperatures $T = 0.8, 1.2$, and 3.0 K (from larger to smaller slope).

experimental data.²

The static structure factor $S(q)$ is the zero energy-weighted sum rule of the dynamic response (Eq. 9). This function can be exactly calculated using the PIMC method as it is the value of the imaginary-time intermediate scattering function at $\tau = 0$. In Fig. 11, we show results of $S(q)$ for the range of analyzed temperatures. The effect of the temperature on the position and height of the main peak is quite small, in agreement with the x-ray experimental data from Ref. 37. We observe a small displacement of the peak to larger q values and a simultaneous decrease of the height when T increases. These effects can be mainly associated to the decrease of the density along SVP when the temperature grows. For values $q \lesssim 0.5 \text{ \AA}^{-1}$ we do not have available data due to the finite size of our simulation box. Therefore, we can not reach the zero momentum value which is related to the isothermal compressibility χ_T through the exact relation

$$S(q=0) = \rho k_B T \chi_T, \quad (14)$$

with k_B the Boltzmann constant and ρ the density. The requirement of this condition produces that $S(q)$ starts to develop a minimum around $q \simeq 0.5 \text{ \AA}^{-1}$ when T increases. Our results also show this feature but for larger T (~ 3.6 K) than in experiments (~ 3 K) due to our lack of data at low q .

From the dynamic structure factor, we can calculate the static response function $\chi(q)$ since this is directly

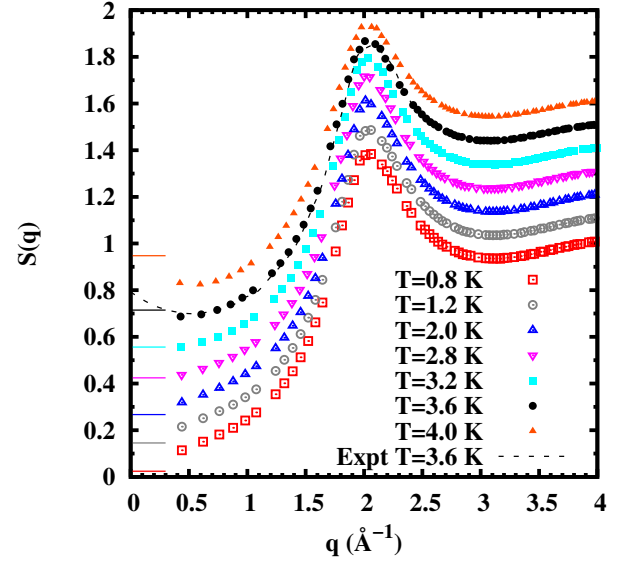


FIG. 11. (Color online) Static structure factor $S(q)$ at different temperatures across T_λ . The results have been shifted vertically a constant value to make its reading easier. The dashed line stands for experimental data from Ref. 37. Short horizontal lines at $q = 0$ correspond to the value (Eq. 14) obtained from PIMC.

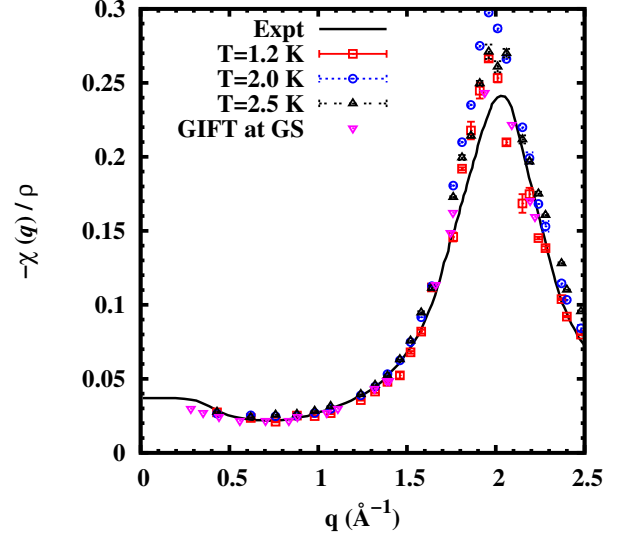


FIG. 12. (Color online) Static response function at $T = 1.2, 2.0$, and 2.5 K. For comparison, we also report zero-temperature QMC results²¹ and experimental data obtained at $T = 1.2$ K.^{35,36}

related to the $1/\omega$ sum rule through the relation

$$\chi(q) = -2\rho \int_{-\infty}^{\infty} d\omega \frac{S(q, \omega)}{\omega} = -2\rho m_{-1}. \quad (15)$$

The dominant contribution to the m_{-1} sum rule is the quasi-particle peak and thus it is less sensitive to the multi-phonon part.³⁸ In Fig. 12, we report the results

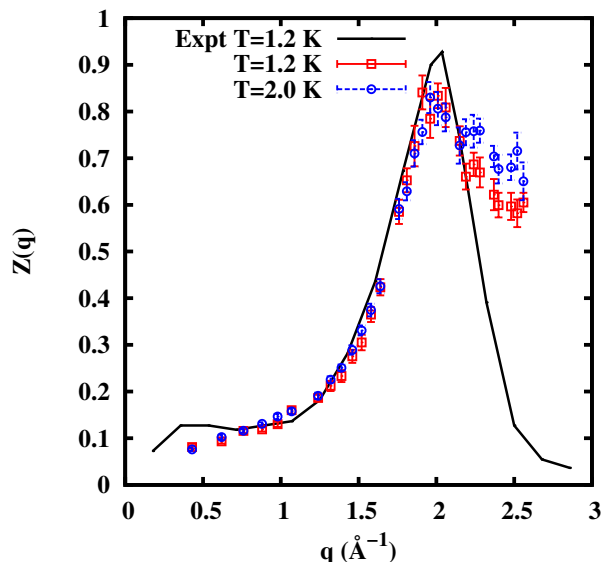


FIG. 13. (Color online) One-phonon contribution to the dynamic response, $Z(q)$, at different temperatures. Experimental results at $T = 1.2$ K from Refs. 35 and 36.

obtained for $\chi(q)$ at temperatures 1.2, 2.0, and 2.5 K. We observe that at low q the effect of T is negligible but around the peak, $q \simeq 2 \text{ \AA}^{-1}$, is really large. In the superfluid regime, the height of the peak clearly increases with T , a feature that has not been reported previously neither from theory nor from experiment. At $T = 2.5$ K, in the normal phase, the main peak decreases again in agreement with the absence of the roton. In the figure, we plot experimental data^{35,36} at $T = 1.2$ K which is close to our result at low q but with less strength in the peak. Results from QMC at zero temperature from Ref. 21 are in an overall agreement with ours at the lowest T , but somehow ours have a slightly higher peak.

The dynamic response of liquid ^4He is usually written as the sum of two terms,

$$S(q, \omega) = S_1(q, \omega) + S_m(q, \omega), \quad (16)$$

where $S_1(q, \omega)$ stands for the sharp quasi-particle peak and $S_m(q, \omega)$ includes the contributions from scattering of more than one phonon (multiphonon part). The intensity (area) below the sharp peak is the function $Z(q)$ which we report in Fig. 13. Our results are compared with experimental data at $T = 1.2$ K from Refs. 35 and 36. As we commented previously, our quasi-particle peaks are less sharp than the experimental ones due to the uncertainties in the inversion problem from imaginary time to energy. However, the area below the peak is not so far from the experimental outcomes. Up to the maximum of the peak, our results are compatible with the experimental function. However, our data lead to a peak with less strength and after that, for larger momenta, our results scatter significantly due to the difficulties in the determination of the area below the peak.

The uncertainties in the area estimation do not allow for the observation of an enhancement of the peak's height when T increases, as reported in experiments.³⁸

IV. CONCLUSIONS

We have carried out PIMC calculations of liquid ^4He in a wide range of temperatures across the normal-superfluid transition T_λ to calculate the imaginary-time intermediate scattering function $F(q, \tau)$. From these functions one can in principle access to the dynamic response $S(q, \omega)$ through an inverse Laplace transform. But this is an ill-conditioned problem that can not be solved to deal with a unique solution. In recent works,²¹ it has been shown that the use of stochastic optimization tools can produce results with a richer structure than previous attempts relying on the maximum entropy method.¹⁷ We have adopted here the well-known simulated annealing technique to extract the dynamic response, without any a priori bias in the search in order to get a result as unbiased as possible. In spite of the lack of any constraint in the cost function, we have verified that the three lowest energy-weighted sum rules are satisfactorily satisfied giving us some confidence on the reliability of our algorithm.

The results of the dynamic response are still not enough sharp in the quasi-particle peaks of the superfluid phase but the position of the peaks and the area below them are in nice agreement with experimental data. Interestingly, our results show clearly the signature of the transition in the roton peak, whose amplitude drops rapidly for $T > T_\lambda$. The effect of the temperature on the phonon-roton spectrum, static structure factor, and static response has been also studied.

The difficulties of extending correlated perturbative approaches to finite T have lead to a really unexplored dynamics of superfluid liquid ^4He , at least from a microscopic approach. With the present work, which can be considered an extension and improvement of a previous work based on the maximum entropy method,²⁷ we have shown that the combination of PIMC and stochastic reconstruction is able to produce a satisfactory description of the quantum dynamics at finite temperature. We are also convinced that in the near future we can improve even more the present results. In this respect, one of the more promising avenues could be the estimation of complex-time correlation functions, instead of the merely imaginary ones, which can reduce the ill-posed character of the inversion problem due to its non-monotonic structure.²²

ACKNOWLEDGMENTS

This research was supported by MICINN-Spain Grant No. FIS2014-56257-C2-1-P.

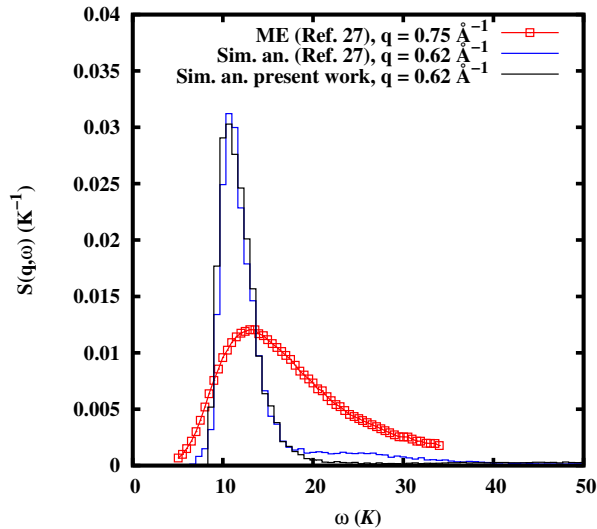


FIG. 14. (Color online) Comparison between the dynamic response obtained with ME and our stochastic optimization method using intermediate scattering data from Ref. 27.

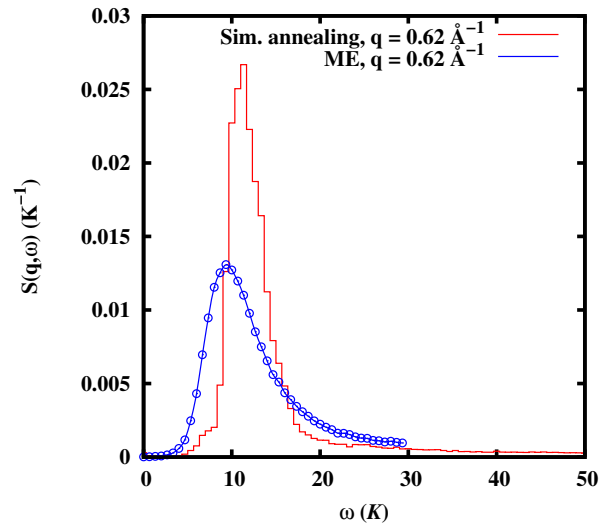


FIG. 15. (Color online) Comparison between the dynamic response obtained with ME and our stochastic optimization method using our intermediate scattering data.

APPENDIX

In Fig. 3, we have compared results for $S(q, \omega)$ derived from our stochastic optimization method and results reported in Ref. 27 using ME. As the intermediate scattering function $F(q, \tau)$ used in both estimations is different and used by different authors it could happen that the differences observed in Fig. 3 were due more to the differences between the calculated imaginary-time response than to the inversion method itself. To clarify this point, we report in this Appendix results of two additional comparisons.

In Fig. 14, we report results for $S(q, \omega)$ at $q = 0.62 \text{ \AA}^{-1}$ using our imaginary-time data and stochastic optimization. In the figure, we also show the dynamic response that we have obtained by applying our inversion method to the imaginary-time data reported in Ref. 27. Finally, the figure also shows the ME results reported in Ref. 27 but for a slightly different q value since results for $q = 0.62 \text{ \AA}^{-1}$ are not given in that paper. As one can see, starting from their published data and applying our method the results compare favorably with our response $S(q, \omega)$. Therefore, the different quality of the input data is so small that no effect is observed.

In order to make a more clear comparison between both inversion methods we show in Fig. 15 results for the dynamic response using our data for $F(q, \tau)$. At the same q value than in Fig. 14, we report results obtained with stochastic optimization and using the ME method. The results are similar to the ones shown in Fig. 14 and lead to the same conclusion, that is, the ME method generates smoother functions than our method. This conclusion is in agreement with a similar analysis reported by Vitali *et al.*²¹.

-
- * jordi.boronat@upc.edu
- ¹ S. W. Lovesey, *Condensed Matter Physics: dynamic correlations* (Benjamin-Cummings, San Francisco, 1986).
 - ² Henry R. Glyde, *Excitations in Liquid and Solid Helium* (Oxford University Press, Oxford, 1994).
 - ³ M. H. Anderson, J. R. Ensher, M. R. Matthews, C. E. Wieman, and E. A. Cornell, *Science* **269**, 198 (1995).
 - ⁴ K. B. Davis, M. O. Mewes, M. R. Andrews, N. J. van Druten, D. S. Durfee, D. M. Kurn, and W. Ketterle, *Phys. Rev. Lett.* **75**, 3969 (1995).
 - ⁵ K. H. Andersen, W. G. Stirling, R. Scherm, A. Stunault, B. Fåk, H. Godfrin, and A. J. Dianoux, *J. Phys.: Condens. Matter* **6**, 821 (1994).
 - ⁶ B. Fåk and J. Bossy, *J. Low Temp. Phys.* **112**, 1 (1998).
 - ⁷ H. R. Glyde, M. R. Gibbs, W. G. Stirling, and M. A. Adams, *Europhys. Lett.* **43**, 422 (1998).
 - ⁸ M. R. Gibbs, K. H. Andersen, W. G. Stirling, and H. Schober, *J. Phys.: Condens. Matter* **11**, 603 (1999).
 - ⁹ J. V. Pearce, R. T. Azuah, B. Fåk, A. R. Sakhel, H. R. Glyde, and W. G. Stirling, *J. Phys.: Condens. Matter* **13**, 4421 (2001).
 - ¹⁰ A. R. Sakhel and H. R. Glyde, *Phys. Rev. B* **70**, 144511 (2004).
 - ¹¹ A. Fabrocini, S. Fantoni, and E. Krotscheck, *Introduction to Modern Methods of Quantum Many-Body Theory and their Applications*, Advances in Quantum Many-Body Theory, Vol. 7 (World Scientific, Singapore, 2002).
 - ¹² C. E. Campbell, E. Krotscheck, and T. Lichtenegger, *Phys. Rev. B* **91**, 184510 (2015).
 - ¹³ K. Beauvois, C. E. Campbell, B. Fåk, H. Godfrin, E. Krotscheck, H. J. Lauter, T. Lichtenegger, J. Ollivier, and A. Sultan (unpublished).
 - ¹⁴ J. Boronat, in *Microscopic Approaches to Quantum Liquids in Confined Geometries*, edited by E. Krotscheck and J. Navarro (World Scientific, Singapore, 2002), pp. 21-90.
 - ¹⁵ D. M. Ceperley, *Rev. Mod. Phys.* **67**, 279 (1995).
 - ¹⁶ J. Kaipio and E. Somersalo, *Statistical and Computational Inverse Problems* (Springer-Verlag, New York, 2004).
 - ¹⁷ M. Jarrell and J. E. Gubernatis, *Phys. Rep.* **269**, 133 (1996).
 - ¹⁸ A. Sandvik, *Phys. Rev. B* **57**, 10287 (1998).
 - ¹⁹ A. S. Mishchenko, N. V. Prokof'ev, A. Sakamoto, and B. V. Svistunov, *Phys. Rev. B* **62**, 6317 (2000).
 - ²⁰ N. V. Prokof'ev and B. V. Svistunov, *JETP Lett.* **97**, 747 (2013).
 - ²¹ E. Vitali, M. Rossi, L. Reatto, and D.E. Galli, *Phys. Rev. B* **82**, 174510 (2010).
 - ²² R. Rota, J. Casulleras, F. Mazzanti, and J. Boronat, *J. Chem. Phys.* **142**, 114114 (2015).
 - ²³ A. N. Tikhonov, *Soviet Math. Dokl.* **4**, 1035 (1963).
 - ²⁴ A. Roggero, F. Pederiva, and G. Orlandini, *Phys. Rev. B* **88**, 094302 (2013).
 - ²⁵ P. Kevin MacKeown, *Stochastic Simulation in Physics* (Springer, Singapore, 1997).
 - ²⁶ A. Nakayama and N. Makri, *PNAS* **102**, 4230 (2005).
 - ²⁷ M. Boninsegni and D.M. Ceperley, *J. Low Temp. Phys.* **104**, 339 (1996).
 - ²⁸ Siu A. Chin and C. R. Chen, *J. Chem. Phys.* **117**, 1409 (2002).
 - ²⁹ K. Sakkos, J. Casulleras, and J. Boronat, *J. Chem. Phys.* **130**, 204109 (2009).
 - ³⁰ M. Boninsegni, N. V. Prokof'ev, and B. V. Svistunov *Phys. Rev. E* **74**, 036701 (2006).
 - ³¹ R. A. Aziz, F.R. W. McCourt, and C. C. K. Wong, *Mol. Phys.* **61**, 1487 (1987).
 - ³² Private communication of K. H. Andersen, taken from Ref. 27.
 - ³³ F. Mezei, *Phys. Rev. Lett.* **44**, 1601 (1980).
 - ³⁴ L. D. Landau and I. M. Khalatnikov, *Zh. Eksp. Teor. Fiz.* **19**, 637 (1949) [*Sov. Phys. JETP* **12**, 216 (1948)].
 - ³⁵ R. A. Cowley and A. D. B. Woods, *Can. J. Phys* **49**, 177 (1971).
 - ³⁶ A. D. B. Woods and R. A. Cowley, *Rep. Prog. Phys.* **36**, 1135 (1973).
 - ³⁷ E. C. Svensson, V. F. Sears, A. D. Woods, and P. Martel, *Phys. Rev. B* **21**, 3638 (1980).
 - ³⁸ F. Caupin, J. Boronat, and K. H. Andersen, *J. Low Temp. Phys.* **152**, 108 (2008).